Extended Phase Shift Control in Dual Active Bridge Converter Considering Magnetizing Inductance of Transformer

Masood Soleimanifard
Department of Electrical Engineering
Tarbiat Modares University
Tehran, Iran
m.soleimanifard@modares.ac.ir

Ali Yazdian Varjani
Department of Electrical Engineering
Tarbiat Modares University
Tehran, Iran
yazdian@modares.ac.ir

***Abstract*—The single phase shift (SPS) method is the conventional switching strategy for the dual active bridge (DAB) structure. Another switching method is the extended phase shift (EPS) method. In this modulation, the zero voltage switching (ZVS) range increases. In this paper, the effect of the magnetizing inductance of the transformer on the output power value and ZVS range with the EPS control method is studied. Simulation results show correctness of the theoretical analysis.**

Keywords—dual active bridge, zero voltage switching, extended phase shift, magnetizing inductance

I. INTRODUCTION

A Dual active bridge (DAB) converter is a bidirectional topology and has benefits including isolation between two sides of the converter, zero voltage switching (ZVS) property, and high power density [1]. A DAB converter can be used for power transfer from grid-to-vehicle and vice versa [2]. Other applications of the DAB converter are energy storage systems [3] and microgrid applications [4].

Fig. 1. shows a DAB converter. References [5], [6] present the DAB topology analysis in the single phase shift (SPS) method. An outer phase shift is between V_P and V_S. When power is transferred from V_1 to V_2 (forward power flow), V_P leads V_S, and when the direction of the power flow changed, V_S leads V_P [7].

To increase the ZVS range, extended phase shift (EPS) modulation is used instead of the SPS method [8], [9]. There are the inner and outer phase shifts in this method. The outer phase shift is between gate pulses of the bridge F_1 and F_2. If $V_1 \geq (V_2/n)$, the inner phase shift is between gate pulses of S_1 and S_4 (or S_2 and S_3), and when $V_1 < (V_2/n)$, it is between gate pulses of S_5 and S_8 (or S_6 and S_7) [10], [11].

In [8]–[12], the DAB converter analysis has been performed with the EPS modulation, but the effect of the magnetizing inductance on the ZVS range and output power has not been investigated (the magnetizing inductance is infinite). In this paper, the magnetizing inductance is considered, and the DAB converter analysis with the EPS modulation is done. Also, the output power and the ZVS range are calculated by considering the magnetizing inductance.

In this paper, in section II, the analysis of the EPS control method is discussed. The effect of the magnetizing inductor on the output power and ZVS range is presented in the next section. Finally, simulation results are given.

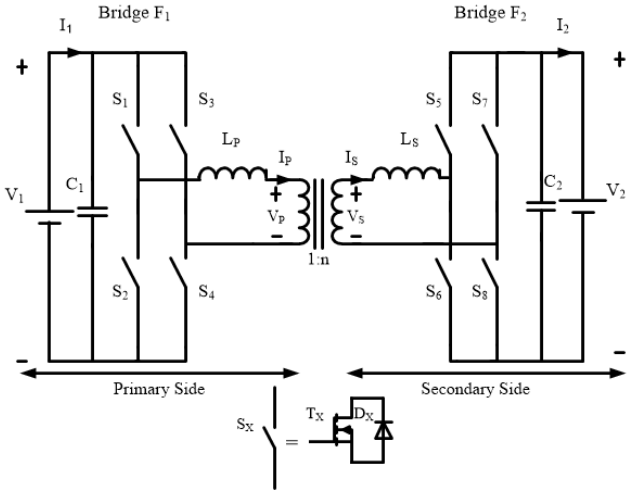

Fig. 1. DAB converter

II. OPERATION MODES WITH EPS CONTROL

In the buck mode ($V_1 \geq (V_2/n)$), DAB topology operating waveforms and gate pulses of switches with the SPS method are shown in Fig. 2, where $V_S' = V_S/n$, $V_2' = V_2/n$ and $\omega = 2\pi f_s$ (f_s is the switching frequency). In this switching control strategy, D is the outer phase shift. The sign of D and its value indicate the direction and amount of the power flow, respectively.

Fig. 3 shows the DAB converter operating waveforms and gate pulses of the switches with the EPS method in the buck mode [10]. In Fig. 3 (a), the gate pulse of S_1 leads S_5, where $0 \leq (d_1 + d_2) \leq 1$, $0 \leq d_1 \leq 1$,and $0 \leq d_2 \leq 1$ (Mode 1). In Fig. 3 (b), the gate pulse of S_5 leads S_1, where $0 \leq d_2 \leq d_1 \leq 1$ (Mode 2). d_1 and d_2 are inner and outer phase shifts, respectively. Fig. 4 shows DAB topology operating waveforms with the EPS control method, when $V_1 < (V_2/n)$ (boost mode) [10]. In Fig. 4 (a), the gate pulse of S_1 leads S_5, and $0 \leq (d_1 + d_2) \leq 1$, $0 \leq d_1 \leq 1$, and $0 \leq d_2 \leq 1$ (Mode 3). In Fig. 4 (b), the gate pulse of S_5 leads S_1 and $0 \leq d_2 \leq d_1 \leq 1$ (Mode 4). D_φ is the phase shift between V_P and V_S'. To reduce the circulating currents, D_φ is not more than $\pi/2$ [13]. Therefore, in addition to the above conditions, in modes 1 and 3, $d_1 + 2d_2 \leq 1$. In this paper, the forward direction of the power flow is analyzed (positive power flow). For the reverse direction, states of switches in the bridge F_1 and bridge F_2 are exchanged, and a similar analysis can be done [5].

In this section, the magnetizing inductance is considered, and the mathematical analysis is presented with the EPS control. Fig. 5 shows the primary referred model of

2021 29th Iranian Conference on Electrical Engineering (ICEE) | 978-1-6654-3365-5/21/$31.00 ©2021 IEEE | DOI: 10.1109/ICEE52715.2021.9544138

Authorized licensed use limited to: Electricity Generating Authority of Thailand. Downloaded on December 01,2021 at 07:51:13 UTC from IEEE Xplore. Restrictions apply.

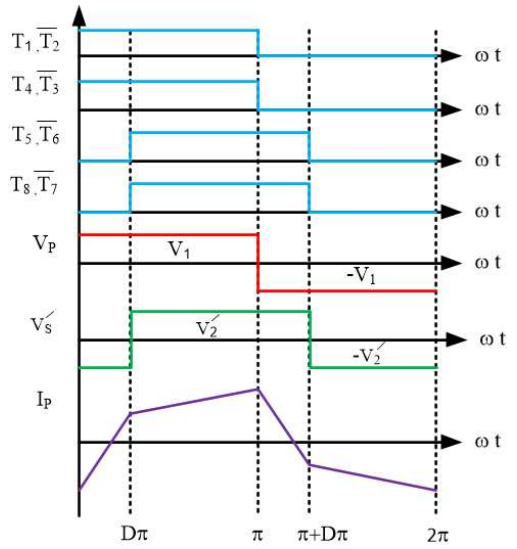

Fig. 2. DAB topology operating waveforms in the buck state with the SPS method

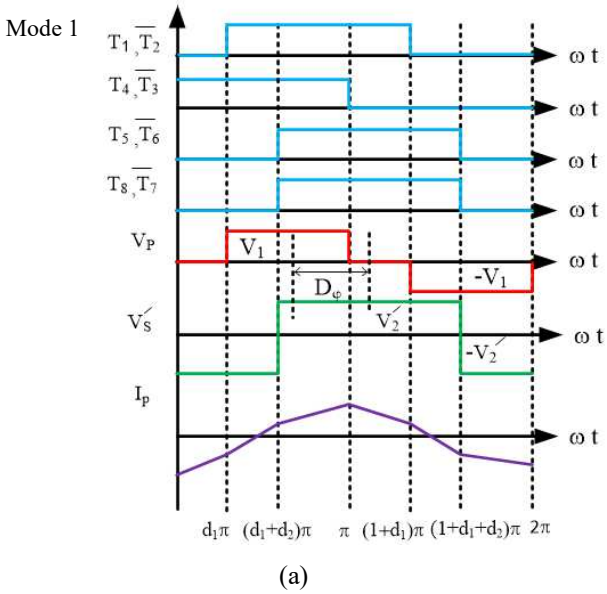

(a)

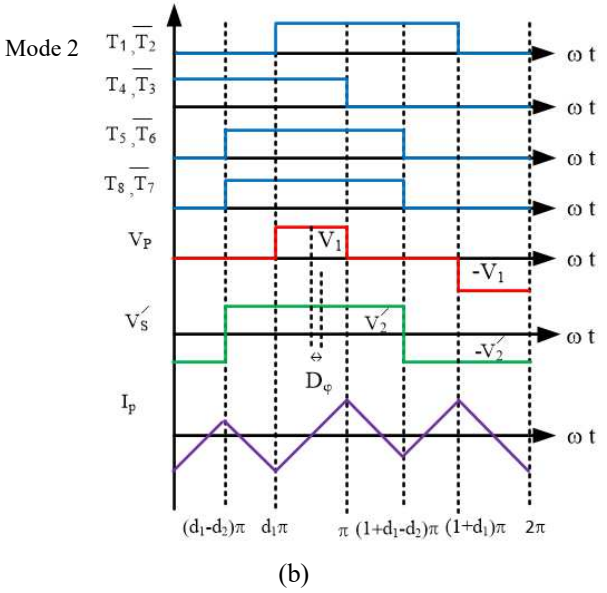

(b)

Fig. 3. DAB topology operating waveforms in the buck state with the EPS method (a) S_1 leads S_5 (b) S_5 leads S_1

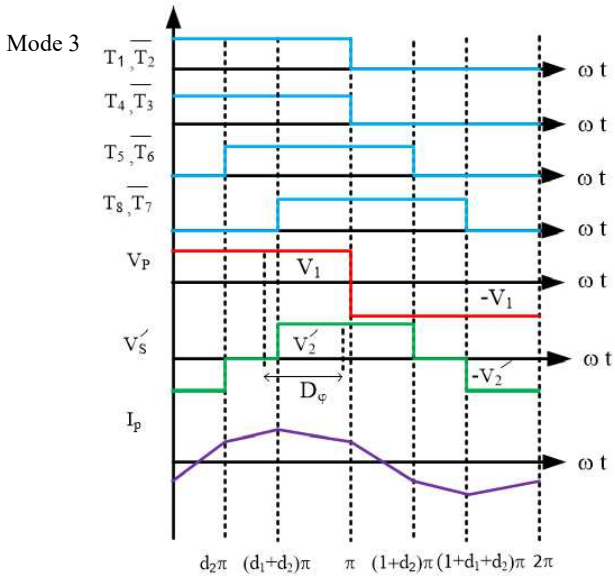

(a)

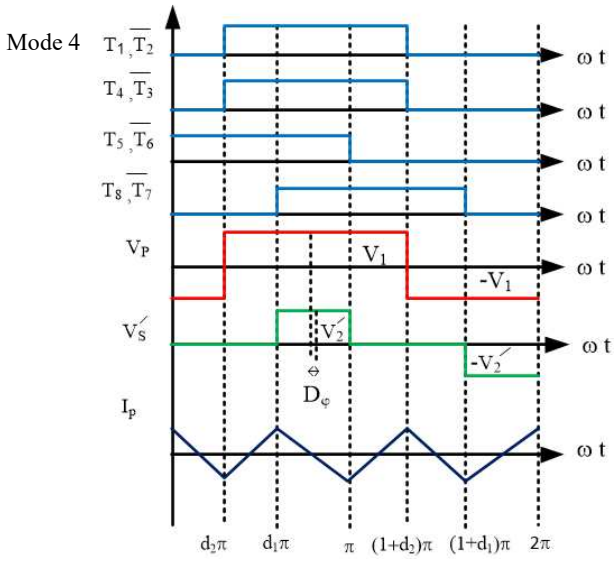

(b)

Fig. 4. DAB topology operating waveforms in the boost state with the EPS method (a) S_1 leads S_5 (b) S_5 leads S_1

the DAB topology. L is the leakage inductance and L_M is the magnetizing inductance. According to Fig. 5, I_P and I_S' can be calculated from the following equations.

$$\frac{dI_P}{d\theta} = A'V_P - BV_S' \quad (1)$$

$$\frac{dI_S'}{d\theta} = BV_P - AV_S' \quad (2)$$

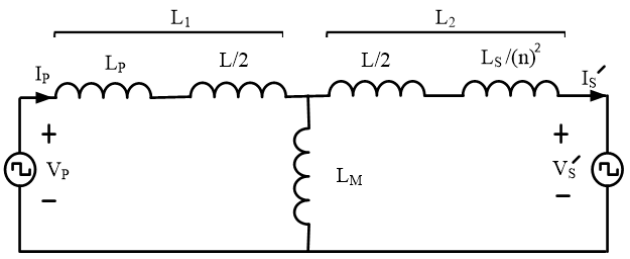

Fig. 5. Primary referred model of the DAB converter

Authorized licensed use limited to: Electricity Generating Authority of Thailand. Downloaded on December 01,2021 at 07:51:13 UTC from IEEE Xplore. Restrictions apply.

Where

$$A = \frac{L_1+L_M}{(L_1L_2+L_1L_M+L_ML_2)\omega} \quad (3)$$

$$B = \frac{L_M}{(L_1L_2+L_1L_M+L_ML_2)\omega} \quad (4)$$

$$A' = \frac{L_2+L_M}{(L_1L_2+L_1L_M+L_ML_2)\omega} \quad (5)$$

$$I_S' = nI_S \quad (6)$$

$$\theta = \omega t \quad (7)$$

In Fig. 5, the average current of inductors in a cycle must be zero [6]. Therefore, using (1)–(2), in different modes, the transformer primary and secondary currents are shown in Tables I and II, respectively. Due to the half-wave symmetry, current equations are given in a half cycle.

III. Effect of the Magnetizing Inductance on the Output Power and ZVS Range

In this section, the output power and ZVS range of the DAB structure are calculated using the analysis performed in section II.

A. Effect of the Magnetizing Inductance on the Output Power

The output power (P) is expressed as

Modes 1 and 3:

$$P = \frac{\pi}{4}BV_1V_2'(2d_1 + 4d_2 - 2d_1^2 - 4d_2^2 - 4d_1d_2) \quad (8)$$

Modes 2 and 4:

$$P = \frac{\pi}{2}BV_1V_2'(1-d_1)(d_1-2d_2) \quad (9)$$

According to (9) in modes 2 and 4, if the following relation exists, the output power is positive.

$$d_1 \geq 2d_2 \quad (10)$$

Fig. 6 shows the output power in per-unit versus d_2 for

TABLE I. Primary Current of the Transformer

Mode	I_P
Mode 1	$I_P(0) = \frac{A'\pi V_1(d_1-1) + B\pi V_2'(1-2d_1-2d_2)}{2}$ $I_P(d_1\pi) = \frac{A'\pi V_1(d_1-1) + B\pi V_2'(1-2d_2)}{2}$ $I_P((d_1+d_2)\pi) = \frac{A'\pi V_1(2d_2+d_1-1) + B\pi V_2'}{2}$
Mode 2	$I_P(0) = \frac{A'\pi V_1(d_1-1) + B\pi V_2'(1-2d_1+2d_2)}{2}$ $I_P((d_1-d_2)\pi) = \frac{A'\pi V_1(d_1-1) + B\pi V_2'}{2}$ $I_P(d_1\pi) = \frac{A'\pi V_1(d_1-1) + B\pi V_2'(1-2d_2)}{2}$
Mode 3	$I_P(0) = \frac{-A'\pi V_1 + B\pi V_2'(1-d_1-2d_2)}{2}$ $I_P(d_2\pi) = \frac{A'\pi V_1(2d_2-1) + B\pi V_2'(1-d_1)}{2}$ $I_P((d_1+d_2)\pi) = \frac{A'\pi V_1(2d_1-1+2d_2) + B\pi V_2'(1-d_1)}{2}$
Mode 4	$I_P(0) = \frac{A'\pi V_1(2d_2-1) + B\pi V_2'(1-d_1)}{2}$ $I_P(d_2\pi) = \frac{-A'\pi V_1 + B\pi V_2'(1-d_1)}{2}$ $I_P(d_1\pi) = \frac{A'\pi V_1(2d_1-1-2d_2) + B\pi V_2'(1-d_1)}{2}$

TABLE II. Secondary Current of the Transformer

Mode	I_S'
Mode 1	$I_S'(0) = \frac{B\pi V_1(d_1-1) + A\pi V_2'(1-2d_1-2d_2)}{2}$ $I_S'(d_1\pi) = \frac{B\pi V_1(d_1-1) + A\pi V_2'(1-2d_2)}{2}$ $I_S'((d_1+d_2)\pi) = \frac{B\pi V_1(2d_2+d_1-1) + A\pi V_2'}{2}$
Mode 2	$I_S'(0) = \frac{B\pi V_1(d_1-1) + A\pi V_2'(1-2d_1+2d_2)}{2}$ $I_S'((d_1-d_2)\pi) = \frac{B\pi V_1(d_1-1) + A\pi V_2'}{2}$ $I_S'(d_1\pi) = \frac{B\pi V_1(d_1-1) + A\pi V_2'(1-2d_2)}{2}$
Mode 3	$I_S'(0) = \frac{-B\pi V_1 + A\pi V_2'(1-d_1-2d_2)}{2}$ $I_S'(d_2\pi) = \frac{B\pi V_1(2d_2-1) + A\pi V_2'(1-d_1)}{2}$ $I_S'((d_1+d_2)\pi) = \frac{B\pi V_1(2d_1-1+2d_2) + A\pi V_2'(1-d_1)}{2}$
Mode 4	$I_S'(0) = \frac{B\pi V_1(2d_2-1) + A\pi V_2'(1-d_1)}{2}$ $I_S'(d_2\pi) = \frac{-B\pi V_1 + A\pi V_2'(1-d_1)}{2}$ $I_S'(d_1\pi) = \frac{B\pi V_1(2d_1-1-2d_2) + A\pi V_2'(1-d_1)}{2}$

different modes and M values. In Fig. 6, it is assumed that $L_1 = L_2 = L'/2$, $L_M = ML'$, and the power base is $V_1V_2'/(L'\omega)$, where L' is a positive value. The output power in modes 1 and 3 is shown in Fig. 6 (a), when $d_1 = 0.1$. In modes 1 and 3, $d_1 + 2d_2 \leq 1$, so $0 \leq d_2 \leq 0.45$. Fig. 6 (b) shows the output power in modes 2 and 4, when $d_1 = 0.6$, so according to (10), $0 \leq d_2 \leq 0.3$. According to (4), as the magnetizing inductance value increases, B increases as well. Thus, according to (8)–(9) in the given operating point by increasing the magnetizing inductance value, the output power increases in all of the modes.

The maximum output power for different modes are obtained from the following equations:

Modes 1 and 3:

$$P_{max} = \frac{\pi}{4}BV_1V_2' \quad (11)$$

Modes 2 and 4:

$$P_{max} = \frac{\pi}{8}BV_1V_2' \quad (12)$$

According to (11)–(12), by increasing the magnetizing inductance value, P_{max} increases as well.

B. Effect of the Magnetizing Inductance on the ZVS Range

To achieve the zero voltage switching, before T_1–T_8 are conducted, the diodes in parallel with them (D_1–D_8) must be conducted [6]. Therefore, the ZVS constraints for the bridge F_1 and F_2 can be obtained, as shown in Table III.

According to Tables I - III, the ZVS condition can be derived as (d is equal to $V_2/(nV_1)$)

Mode 1:

$$\frac{B(1-d_1-2d_2)}{A} < d < \frac{A'(1-d_1)}{B(1-2d_2)} \quad (13)$$

Authorized licensed use limited to: Electricity Generating Authority of Thailand. Downloaded on December 01,2021 at 07:51:13 UTC from IEEE Xplore. Restrictions apply.

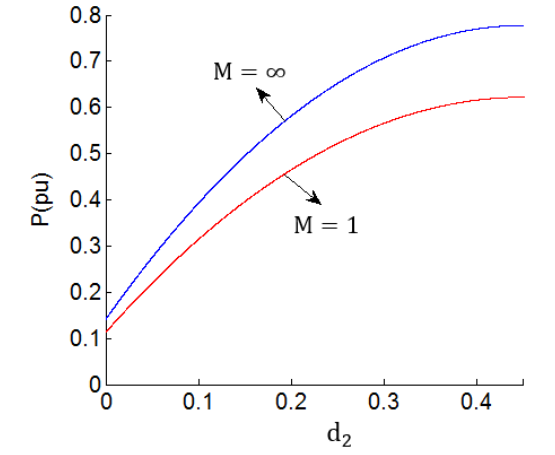

(a)

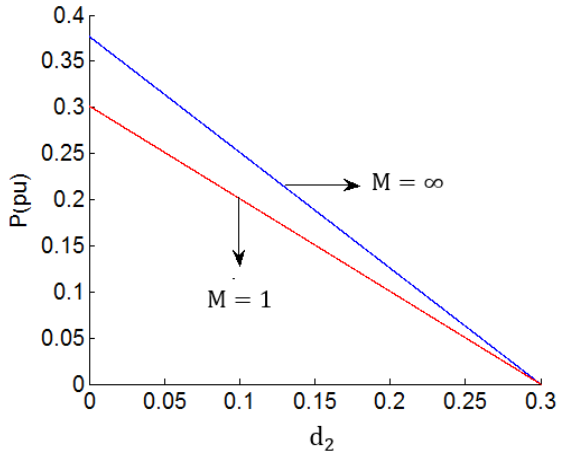

(b)

Fig. 6. Output power versus d_2 (a) Modes 1 and 3 when $d_1 = 0.1$ (b) Modes 2 and 4 when $d_1 = 0.6$

Mode 2:

$$\frac{B(1-d_1)}{A} < d < \frac{A'(1-d_1)}{B(1-2d_2)} \tag{14}$$

Mode 3:

$$\frac{B(1-2d_2)}{A(1-d_1)} < d < \frac{A'}{B(1-2d_2-d_1)} \tag{15}$$

Mode 4:

$$\frac{B(1-2d_2)}{A(1-d_1)} < d < \frac{A'}{B(1-d_1)} \tag{16}$$

According to (3)–(5), as the magnetizing inductor value decreases, (B/A) decreases as well, but (A'/B) increases. Therefore, using (13)–(16), it can be seen that for the given d_1 and d_2, by decreasing the magnetizing inductance value, the ZVS conditions are provided in the wider range of d. For example, the ZVS regions for different modes and two values of M ($M = 1, M = \infty$) are shown in Fig. 7 and Fig. 8 as a function of d_2 and d. It is assumed that $L_1 = L_2 = \frac{L'}{2}$ and $L_M = ML'$ (L' is a positive value). Fig. 7 (a) and (b) show ZVS regions for modes 1 and 3, respectively, when $d_1 = 0.1$. ZVS regions for modes 2 and 4 are shown in Fig. 8 (a) and (b), respectively, when $d_1 = 0.6$. According to Fig. 7 and Fig. 8, when M is equal to one, ZVS can be obtained in a wider range of d compared to $M = \infty$.

TABLE III. ZVS CONSTRAINTS FOR THE BRIDGE F_1 AND F_2

Mode	bridge F_1	bridge F_2
Mode 1	$I_P(d_1\pi) < 0$	$I'_S((d_1+d_2)\pi) > 0$
Mode 2	$I_P(d_1\pi) < 0$	$I'_S((d_1-d_2)\pi) > 0$
Mode 3	$I_P(0) < 0$	$I'_S(d_2\pi) > 0$
Mode 4	$I_P(d_2\pi) < 0$	$I'_S(0) > 0$

Therefore, to design the DAB structure with the EPS method, values of the inductors (L_1, L_2, and L_M) must be selected so that according to (8)–(9), the DAB converter can transfer the desired output power value and (13)–(16) are satisfied to achieve the ZVS.

IV. SIMULATION RESULTS

This simulation is performed in mode 1 for two different values of the magnetizing inductance using PSIM software [14]. First, the magnetizing inductance is infinite, and in the next case, the magnetizing inductance is 180 *uH*.

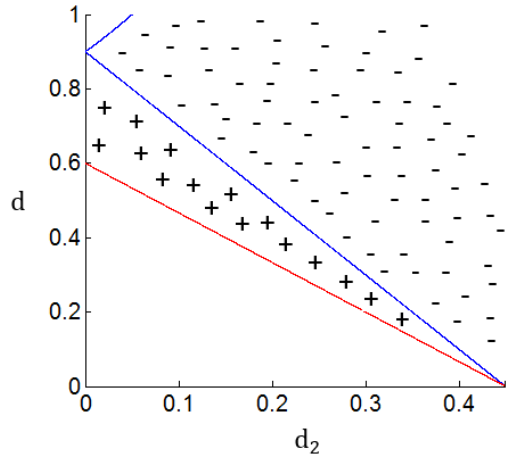

(a)

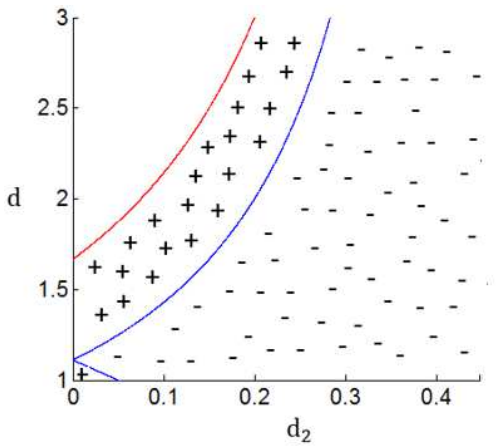

(b)

Fig. 7. ZVS regions when d_1 is 0.1 (a) ZVS regions of mode 1 ($d \leq 1$) (b) ZVS regions of mode 3 ($d > 1$) , '-' : ZVS region for both values of M ($M = 1, M = \infty$), '+': ZVS region only for $M = 1$

Authorized licensed use limited to: Electricity Generating Authority of Thailand. Downloaded on December 01,2021 at 07:51:13 UTC from IEEE Xplore. Restrictions apply.

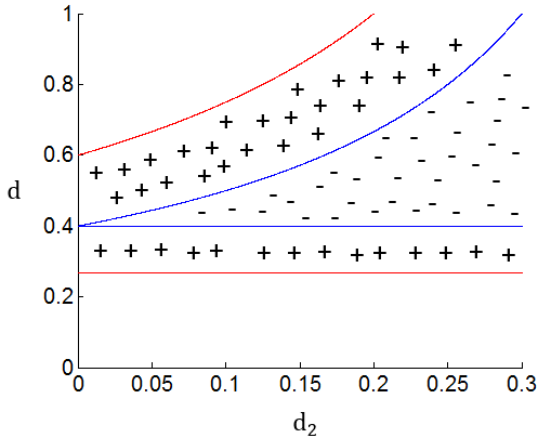

(a)

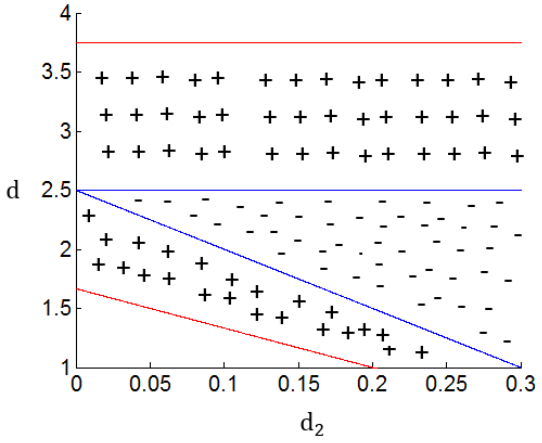

(b)

Fig. 8. ZVS regions when d_1 is 0.6 (a) ZVS regions of mode 2 ($d \leq 1$) (b) ZVS regions of mode 4 ($d > 1$), '-' : ZVS region for both values of M ($M = 1$, $M = \infty$), '+' : ZVS region only for $M = 1$

The simulation parameters are given in Table IV. According to (13), if L_M is less than 314 uH, ZVS occurs. Simulated waveforms are shown in Fig. 9, when L_M is infinite. $I_P(d_1\pi)$ and $I_S((d_1+d_2)\pi)$ are negative, so according to Table III, ZVS can be obtained in T_1–T_4 but it cannot be obtained in T_5-T_8. Fig. 10 shows simulated waveforms, when $L_M = 180\ uH$. $I_P(d_1\pi)$ is negative and $I_S((d_1+d_2)\pi)$ is positive, so ZVS can be obtained in T_1-T_8. In the same conditions, ZVS is achieved by decreasing L_M.

Fig. 11 shows the output current when $L_M = \infty$. $I_2 = 9.12\ Amps$ and $V_2 = 157\ Volts$, so the output power is 1431.84 Watts. Fig. 12 shows the output current, when $L_M = 180\ uH$. The output current and voltage are 8.96 $Amps$ and 157 $Volts$, respectively, so the output power is 1406.72 Watts and it is less than the case where L_M is infinite.

TABLE IV. SIMULATION PARAMETERS

Parameter	Value
d_1	0.1
d_2	0.05
V_{out}	157 V
V_{in}	100 V
n	2
$L_1 = L_2$	6uH
f_s	20 kHz

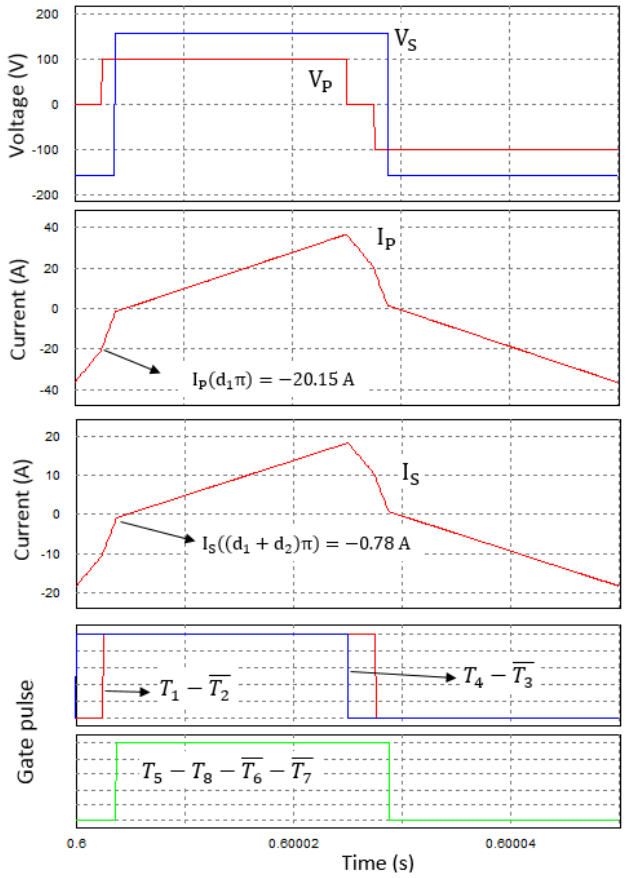

Fig. 9. Simulated waveforms when $L_M = \infty$

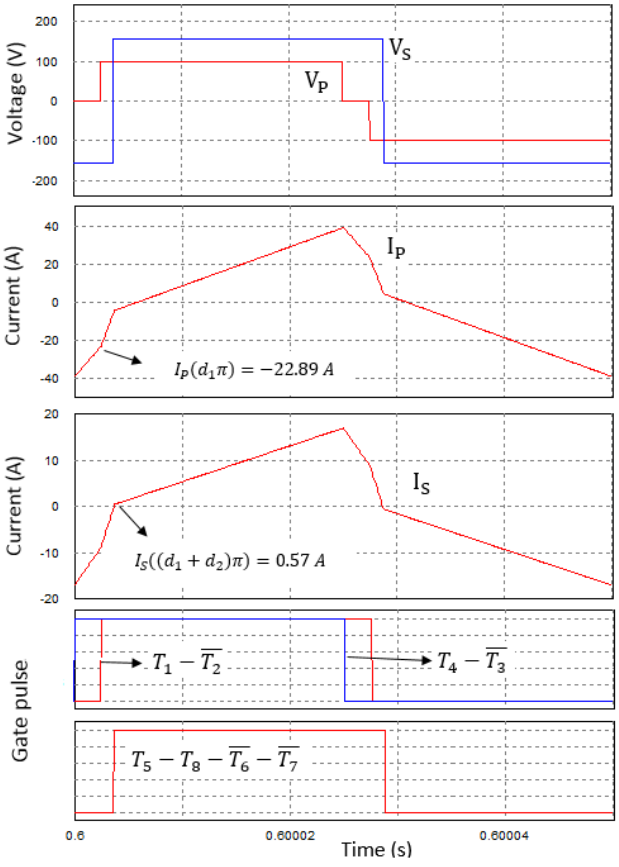

Fig. 10. Simulated waveforms when $L_M = 180\ uH$

Authorized licensed use limited to: Electricity Generating Authority of Thailand. Downloaded on December 01,2021 at 07:51:13 UTC from IEEE Xplore. Restrictions apply.

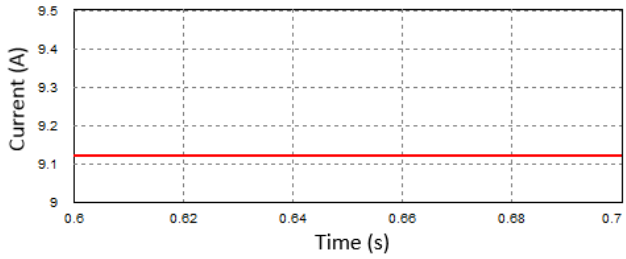

Fig. 11. Output current waveform when $L_M = \infty$

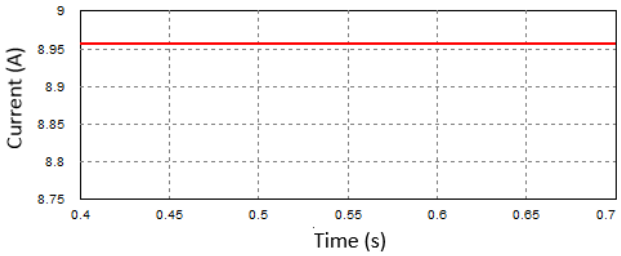

Fig. 12. Output current waveform when $L_M = 180\ uH$

V. Conclusion

The DAB topology analysis with the EPS control method was performed in this paper, and the magnetizing inductance was considered in the equivalent circuit of the transformer. The ZVS range and output power were obtained in all four modes. It was shown that by decreasing the magnetizing inductance, the output power decreases, and in the given d_1 and d_2, ZVS could be obtained in a wider range of d.

References

[1] F. Feng, X. Zhang, F. Lin, and H. B. Gooi, "Impedance modeling and stability analysis of dual active bridge converter with LC input filter," CES Transactions on Electrical Machines and Systems, vol. 2, no. 3, pp. 289-295, 2018.

[2] I. Skouros, A. Bampoulas, and A. Karlis, "A bidirectional dual active bridge converter for V2G applications based on DC microgrid," in 2018 Thirteenth International Conference on Ecological Vehicles and Renewable Energies (EVER), 2018: IEEE, pp. 1-9.

[3] D.-K. Jeong, H.-S. Kim, J.-W. Baek, J.-Y. Kim, and H.-J. Kim, "Dual active bridge converter for Energy Storage System in DC microgrid," in 2016 IEEE Transportation Electrification Conference and Expo, Asia-Pacific (ITEC Asia-Pacific), 2016: IEEE, pp. 152-156.

[4] H. R. Mamede, W. M. dos Santos, R. F. Coelho, and D. C. Martins, "A multicell Dual-Active Bridge converter for increasing the reliability of power supply in a DC microgrid," in 2015 IEEE First International Conference on DC Microgrids (ICDCM), 2015: IEEE, pp. 274-279.

[5] R. Barlik, M. Nowak, and P. Grzejszczak, "Power transfer analysis in a single phase dual active bridge," Bulletin of the Polish Academy of Sciences: Technical Sciences, vol. 61, no. 4, pp. 809-828, 2013.

[6] M. Kheraluwala, R. W. Gascoigne, D. M. Divan, and E. D. Baumann, "Performance characterization of a high-power dual active bridge DC-to-DC converter," IEEE Transactions on industry applications, vol. 28, no. 6, pp. 1294-1301, 1992.

[7] B. Zhao, Q. Song, W. Liu, and Y. Sun, "Overview of dual-active-bridge isolated bidirectional DC–DC converter for high-frequency-link power-conversion system," IEEE Transactions on Power Electronics, vol. 29, no. 8, pp. 4091-4106, 2014.

[8] B. Zhao, Q. Yu, and W. Sun, "Extended-phase-shift control of isolated bidirectional DC–DC converter for power distribution in microgrid," IEEE Transactions on Power Electronics, vol. 27, no. 11, pp. 4667-4680, 2012.

[9] A. Kumar, A. Bhat, and P. Agarwal, "Comparative analysis of dual active bridge isolated DC to DC converter with single phase shift and extended phase shift control techniques," in 2017 6th International Conference on Computer Applications In Electrical Engineering-Recent Advances (CERA), 2017: IEEE, pp. 397-402.

[10] H. Shi et al., "Minimum-backflow-power scheme of DAB-based solid-state transformer with extended-phase-shift control," IEEE Transactions on Industry Applications, vol. 54, no. 4, pp. 3483-3496, 2018.

[11] G. G. Oggier, G. O. Garcia, and A. R. Oliva, "Switching control strategy to minimize dual active bridge converter losses," IEEE Transactions on Power Electronics, vol. 24, no. 7, pp. 1826-1838, 2009.

[12] G. G. Oggier, R. Leidhold, G. O. Garcia, A. R. Oliva, J. C. Balda, and F. Barlow," Extending the ZVS operating range of dual active bridge high-power DC-DC converters," in 2006 37th IEEE Power Electronics Specialists Conference, 2006: IEEE, pp. 1-7.

[13] S. S. Muthuraj, V. Kanakesh, P. Das, and S. K. Panda, "Triple phase shift control of an LLL tank based bidirectional dual active bridge converter," IEEE Transactions on Power Electronics, vol. 32, no. 10, pp. 8035-8053, 2017.

[14] PSIM User Manual, v 9.1, Powersim Inc., 2011.

.

Authorized licensed use limited to: Electricity Generating Authority of Thailand. Downloaded on December 01,2021 at 07:51:13 UTC from IEEE Xplore. Restrictions apply.